Energy Storage Materials 12 (2018) 216–222

Contents lists available at ScienceDirect

Energy Storage Materials

journal homepage: www.elsevier.com/locate/ensm

TiS_2 as a high performance potassium ion battery cathode in ether-based electrolyte

Liping Wang[a], Jian Zou[a], Shulin Chen[b,c], Ge Zhou[d], Jianming Bai[e], Peng Gao[c,*], Yuesheng Wang[d], Xiqian Yu[d,*], Jingze Li[a,*], Yong-Sheng Hu[d], Hong Li[d]

[a] State Key Laboratory of Electronic Thin Films and Integrated Devices, University of Electronic Science and Technology of China, Chengdu 610054, China
[b] State Key Laboratory of Advanced Welding and Joining, Harbin Institute of Technology, Harbin 150001, China
[c] Electron Microscopy Laboratory, and International Center for Quantum Materials, School of Physics, Peking University, Beijing 100871, China
[d] Institute of Physics, Chinese Academy of Sciences, Beijing 100190, China
[e] National Synchrotron Light Source II, Brookhaven National Laboratory, Upton, NY 11973, USA

ARTICLE INFO

Keywords:
Transition metal dichalcogenides
Potassium ion battery
Stage structure
Ether-based electrolyte
Layer structure

ABSTRACT

Potassium ion batteries are potential energy storage devices owing to their low cost and good K^+ diffusion kinetics due to the small Stoke's radius. Here, we report a layered TiS_2 cathode material, demonstrating outstanding potassium storage cycling and rate performances in ether-based electrolyte, with a capacity of 80 mAh g^{-1} at 20 C and 63 mAh g^{-1} after 600 cycles (1.5–3.0 V, corresponding to 4.8 A g^{-1}). The phase transitions during K ion intercalation at the atomic level are explored *via* High Resolution Transmission Electron Microscopy (HRTEM) and *ex-situ* X-ray diffraction (XRD) combined with Rietveld refinements. It undergoes a second-stage structure to be $K_{0.11}TiS_2$ and then first-stage $K_{0.56}TiS_2$. The K cations intercalate into trigonal prismatic sites with a sliding of Ti-S plane by 120 degree-rotation, rendering a $\sqrt{3} \times \sqrt{3}$ commensurate superstructure along the [001] zone. The K stage intercalation is in favor of a Daumas-Hérold model rather than Rüdorff model. This study demonstrates that the layer structure materials are promising candidates for high performances K-ion batteries and highlights the importance of improving electrochemical performances with electrolyte modification.

1. Introduction

In the past decades, lithium ion batteries have achieved tremendous success in applications of portable electronics and electric vehicles owing to the high energy density and extraordinary cycling performance. However, lithium resources present global rareness (20 ppm) and uneven distribution in earth crust. According to the US Geological Survey in 2017, the lithium reserve in the world is approximately 14 million tons, which can only support approximately 1.4 billion Tesla Model S. As a result, exploiting alternative materials with natural abundance and low cost is urgently needed to meet the increasing energy storage demand, especially for large scale applications like grid storage [1,2]. Alkaline metal ion (i.e. Na^+ and K^+) based batteries demonstrate to be promising alternatives due to their chemical similarity to Li. Among them, the K-ion batteries (KIBs) present unique advantages. Most importantly, K crust is 1000 times greater than Li crust in nature, which can well mitigate the resource abundance concern. Despite the larger atomic number, the radius of solvated K cation is smaller than that of Li and Na in solutions, which provides better kinetic response with higher diffusion rate [3]. In our recent study, K intercalation into the potassium terephthalate was demonstrated to deliver higher capacity and superior rate performance than that of Li analogues [4]. K^+ is further proven to be more thermodynamically favorable into the graphite than Na^+ [5]. Additionally, the standard potential for K^+/K is −2.97 V versus standard hydrogen electrode (SHE), which theoretically offers higher operational voltage than Na-ion battery as Na^+/Na is −2.71 V versus SHE. The standard potential of K^+/K is even lower than Li^+/Li (−3.04 V versus SHE) in propylene carbonate-based nonaqueous electrolyte due to the high K^+ desolvation energy [6]. Moreover, the current collector in the prepared cell can be Al instead of Cu as no formation of K-Al alloy at low potential, which is beneficial in the commodity cells for higher energy density and lower cost.

Up to now, there are only limited literature reports on K-ion batteries, most of which are analogues of lithium ion battery electrodes, such as carbon anodes including soft carbon, hard carbon, and graphite [7–9], Prussian blue $KFe^{III}Fe^{II}(CN)_6$ [10], layer metal oxides K_xMO_2(M = Co, Mn) [11], and $K_3V_2(PO_4)_3$ [12]. No superiority in terms of battery

* Corresponding authors.
E-mail addresses: pengg@pku.edu.cn (P. Gao), xyu@iphy.ac.cn (X. Yu), lijingze@uestc.edu.cn (J. Li).

https://doi.org/10.1016/j.ensm.2017.12.018
Received 17 November 2017; Received in revised form 18 December 2017; Accepted 18 December 2017
Available online 19 December 2017

capacity nor cycling performance have been reported in these lithium analogues materials. Furthermore, these electrodes suffer fast capacity decay, making the exploitation of novel materials the key topic in KIBs. Transition metal dichalcogenides MX_2 (M = Ti, Zr, Hf, Ta, V, Nb, Mo, W; X = S, Se, Te et al.) with layered structures enable accommodating Li, Na, Mg, and Ca cations [13–16]. Recently, Tian et al. discovered that chemically prepotassiated TiS_2 ($K_{0.25}TiS_2$) demonstrated improved cycling performance in carbonate-based electrolyte, exhibiting high initial Coulombic efficiency [17]. They further evidenced the phase transformations in TiS_2 during K intercalations *via in-situ* XRD. However, due to the limited XRD collecting range (2 theta range from 11° to 16°) and low intensity of the diffraction peaks except for the (001) peak, detailed phase structures at the atomic level can not be achieved from the *in-situ* XRD patterns.

It is well known that electrolytes with distinguished functional groups, polarities, and molecular sizes have major impacts on battery performance [18,19]. For instance, conventional graphite anode presents much higher power capability in ether-based electrolyte than that in typical carbonate electrolyte system due to the lithium-ether co-intercalation effect [20]. The unusual high rate capability results from the compatibility between electrolyte and electrode, the fast charge-transfer kinetics as well as the absence of solid electrolyte interphases (SEI) in ether-based system [20]. Another example is that the electrochemical performance of Li-S cells using dioxolane (DOL)/dimethoxyethane (DME) co-solvents based electrolyte with high donation number and high Li^+ diffusivity outperformed that of tetramethylene sulfone system [21]. In the research field of KIBs, the reported non-aqueous electrolytes are KPF_6 or KTFSI salts in mixture of carbonate solvents (*e.g.* EC, DMC, PC), as derived from traditional lithium ion battery electrolytes. While little knowledge has been achieved about the KIBs electrodes performance in other electrolyte systems [22,23]. Therefore, it would be intriguing to investigate the impacts of electrolyte (such as ether) on the KIBs system.

In this work, we have carried out detailed and fundamental investigations on the performance of TiS_2 KIBs in ether-based electrolyte, *i.e.*, 1, 2-dimethoxyethane (DME), which demonstrates surprisingly outstanding rate performance despite several phase transitions occur in battery cycling process. According to the Galvanostatic Intermittent Titration Technique (GITT), the K^+ intercalation into the TiS_2 in ether based electrolytes demonstrates a consistent mechanism with that of EC-DMC based electrolyte. More importantly, with the help of HRTEM and *ex-situ* XRD, we have explored the stage structures of TiS_2 cathode and verified the tetragonal prism coordinations of K^+ ions. In the atomic scale level, this particular structure originates from Ti-S plane sliding of 120° for a $\sqrt{3} \times \sqrt{3}$ superstructure formation during K intercalation. In addition, the K^+ intercalation in TiS_2 cathode presents preference for Daumas-Hérold stage model, as evidenced from our high resolution TEM.

2. Experimental section

2.1. Electrodes preparation

Plate shape TiS_2 was purchased from Sigma-Aldrich Company. The TiS_2 electrodes were prepared by a solution-cast method. A slurry of 80 wt% active material TiS_2, 10 wt% acetylene black and 10 wt% PVDF binder in N-methyl-2-pyrrolidine (NMP) solution was casted on Al foil before dried in vacuum at 90 °C for overnight. The weight of the active materials per electrode was about 2 mg cm^{-2}. Potassium metal and glass fiber were used as the anode and the separator, respectively. The electrolyte is KPF_6 salt with concentration of 1 M in 1, 2-dimethoxyethane (DME) solvent. For a comparison, 1.0 M KPF_6 dissolved in EC/DMC (1:1 in volume) was also prepared. 2032-type coin cells were assembled in an argon-filled glove box and the cells were cycled using a CT2001A cell test instrument (LAND Electronic Co.). The cyclic voltammetry (CV) curves were performed at different scan rates using Arbin BT2000 (Arbin Instruments Co. Ltd.) electrochemical workstation. Electrochemical impedance spectroscopy (EIS) measurements were performed at its open circuit voltage before discharging-charging using an electrochemical workstation model CHI660B (CH Instruments Inc.). The amplitude of the a.c. signal was 5 mV over the frequency range of 10^{-2} and 10^5 Hz. All the measurements were carried out at room temperature.

2.2. Materials characterization

The crystal structures of K_xTiS_2 ($0 < x < 1$) were identified by X-ray diffraction using Cu Kα radiation (XRD, λ = 1.54056 Å, X'Pert ProMPD) with a step size of 0.02° (2θ) in the range 10–70°. The patterns were analyzed by the Rietveld method using Fullprof_suite program. TEM and SAED were performed on FEI Tecnai F20 operated at 200 kV. STEM and EDS-mapping were acquired at an aberration-corrected FEI (Titan Cubed Themis G2) operated at 300 kV. The powders scratched from the electrode were dispersed on a TEM grid (with an amorphous carbon-membrane support) before loaded onto a TEM holder and then transferred to the TEM column. Inductively Coupled Plasma Optical Emission Spectrometry (ICP-OES) was conducted using Optima8300 (PerkinElmer) to detect the element ratio of K and Ti. The sample was peeled off from the current collector and soaked in high concentration HCl for 48 h to dissolve K and Ti. Then, deionized water was added into the solution to adjust the concentration.

3. Results and discussion

Fig. 1**a** demonstrates the XRD pattern of pristine TiS_2, which is indexed to be a space group of *P-3m1* (No. 164) with cell parameters of $\boldsymbol{a} = \boldsymbol{b} = 3.409$ Å, $\boldsymbol{c} = 5.703$ Å. It has a highly preferred orientation along (001) lattice plane. Its crystallographic structure along [100] direction is presented in Fig. 1**b**, which is a layer structure along the *c* axis and the layer distance is 5.703 **Å,** equaling to the lattice distance of (001) plane. Every layer consists of two hexagonally close-packed S atoms, where the transition metal Ti locates at the center to form octahedrons. The layers between are connected with van de Waals forces. The obtained pristine TiS_2 powders are in plate shape (Fig. 1**c**) and the plates are single crystals with well crystalline (Fig. 1**d**). In line with the XRD study, the plates have preference of (001) planes evidenced from the STEM.

The electrochemical properties in the voltage window 1.5–3.0 V including cyclic voltammetry (CV), galvanostatic discharge-charge, thermodynamic equilibrium potential (GITT), and rate performance of TiS_2 are evaluated and shown in Fig. 2. Meanwhile, for a comparison, its electrochemical properties as lithium ion battery cathodes are also tested in Fig. S1. In the CV (Fig. 2**a**), several redox couples appear indicating multiple electron transfer steps during the potassium intercalation/deintercalation. Consistent with the CV results, the discharge-charge profiles demonstrate plateaus at identical potentials (Fig. 2**b**). In order to obtain its thermodynamic equilibrium potentials, GITT is performed (Fig. 2**c**), in which there are four main plateaus at 2.49 V, 2.37 V, 2.20 V, and 1.87 V. The multiple operational plateaus and the redox couples have correlations with the charge transfer upon intercalations induced structural changes, such as bond lengths, coordination, and superstructures within layers or new stacking between layers [24]. An identical phenomenon during Li intercalations of TiS_2 (Fig. S1**a**) is observed, although it is commonly believed that the Li^+ intercalation is a solid solution process (Fig. S1**b**) with no phase transitions [25,26]. Its capacity retention behaviors at different rates in different electrolytes including the typical carbonate EC-DMC solvents and the ether based DME solvent are studied (Fig. 2**d-e**). It is found that the DME-type has a much higher capacity and better cycling performance than EC-DMC type one. In details, it offers an initial discharge capacity of 134 mAh g^{-1} to be 91 mAh g^{-1} after 100 cycles at

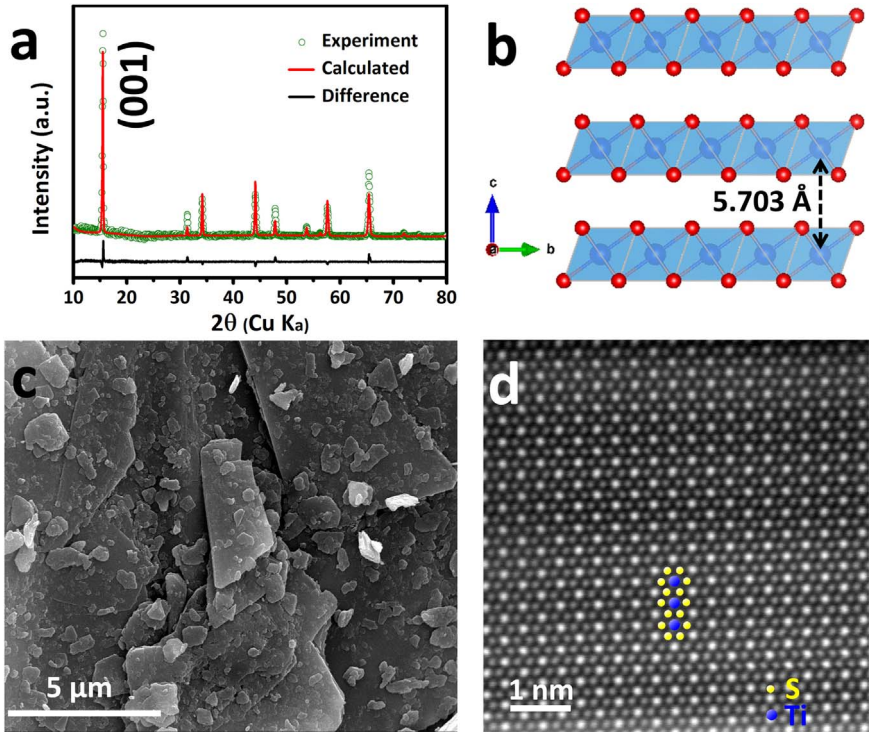

Fig. 1. (a) XRD pattern of TiS_2 powders. (b) Crystallographic structure of TiS_2 along the [100] direction. The Ti, S atoms are denoted by blue, red balls, respectively. (c) SEM image of TiS_2 powders. (d) STEM image of TiS_2 seen from [001] zone axis showing the arrangement of Ti (blue) and S (orange) atoms locating at different hexagonal positions. (For interpretation of the references to color in this figure legend, the reader is referred to the web version of this article).

a current density of 0.48 A g^{-1} (*vs.* 103 mAh g^{-1} at 1st cycle to 19 mAh g^{-1} at 100th cycle in the carbonate system). At a higher current rate of 20 C (4.8 A g^{-1}), the ether cell is remarkably robust having a capacity of 80 mAh g^{-1} at initial to 63 mAh g^{-1} at 600th cycle. In contrast, the carbonate-based cell gives almost no capacity at such high current rate presumably due to kinetic limitations. It is rewarding to note that such capacity at this rate thanks to the plate shape with nanometer thickness and is superior to the reported K ion cathodes (Table S1), *e.g.* MoS_2 [27], $KTi_2(PO_4)_3$ [28], Prussian blue (PB) [10], $KFeSO_4F$ [29], $K_{0.6}CoO_2$ [30]. Meanwhile, we have also extended the voltage window into 1.0–3.0 V for the ether based electrolyte (Fig. S2). The extended operational window causes capacity decay, presumably as a result of uncoverable structure changes as the TiS_2 host needs to accommodate more K ions.

To shed light on the electrolyte effect on the electrochemical properties of TiS_2, GITT measurement for the EC-DMC system is also performed (Fig. 3**a**). The K insertion into the TiS_2 shares the same mechanism with the DME-type as they have the same operational potentials, which can be clearly seen with a normalized capacity as well (Fig. S3**a**). The only difference is that the over-potentials in the carbonate system, normally termed as polarizations, are larger than that in the ether one, which also embodies in their cyclic voltammetry curves under the same scan rate (Fig. S3**b**). The polarizations are combinations of ohm polarizations correlated with the internal resistance, electrochemical reaction polarizations originating from charge transfer resistance, and concentration polarizations rooting in the ion diffusion. The EIS spectroscopies (Fig. 2**b-c**) reveal that the charge-transfer resistance (R_{ct}) in the EC/DMC cell at pristine state is about two magnitude orders larger than that in the DME cell (< 10 Ω). Moreover, the R_{ct} in carbonate-type cell continuously increases with cycling while it remains virtually unchanged in ether-type one. Note that in the voltage window 1.5–3.0 V, there is no solid electrolyte interfaces (SEI) information in the EIS and it is further confirmed with TEM studies which will be shown in the later section. As the K cations need travel in the solid state TiS_2, the K^+ diffusion rate would be the rate-determine step. Consequently, the K ion diffusion obeys the Randles-Sevcik equation [31]. In our CV study, the peak currents are proportional to the square root of the scan rate (Fig. 3**d-f**), indicating the potassiation is a diffusion-control step. A higher slope in the DME system expresses a higher apparent K-ion diffusion coefficient (Fig. 3**f**). In words, both of EIS and CV results reveal that the DME electrolytes provide better kinetics including charge-transfer rates and K ion diffusion rates. It is explained that the linear molecular DME has a higher electron donation number than EC-DMC (20 in DME vs. ~ 16) [32], which is much easier to have interactions with the K ions so as to modify electrolyte-K^+ polarity and diffusivity for better kinetics. As a consequence, high ion mobility in terms of charge-transfer and diffusivity in the interlayer space guarantees a faster ion-exchange reaction with the ambient electrolyte solutions. Here we need also to mention that the DME would aid in improving the potassium metal anode-electrolyte interface. Further detailed investigations are still needed to understand the mechanisms.

To study the phase transitions at an atomic level, we performed *ex-situ* XRD with Rietveld refinement and TEM. The structural evolution as a function of K concentration determined from the capacity is presented in Fig. 4**a-b**. The crystallographic structures for the discharge state $K_{0.56}TiS_2$ at 1.5 V (first-stage structure, ICP stoichiometry: $K_{0.59}TiS_2$) and the charge state $K_{0.11}TiS_2$ at 3.0 V (second-stage structure, ICP stoichiometry: $K_{0.10}TiS_2$) are demonstrated in Fig. 4**c** and their corresponding lattice parameters and atomic occupation details are provided in Table S2 and Fig. S4. It is worth mentioning that the K intercalations into the TiS_2 phase are homogeneous as shown in their elemental mappings (Figs. S5 and 6). As revealed from Fig. 4**b-c**, in the early stage of K intercalation ($0 < x < 0.19$), the pristine phase rapidly transforms into a metastable single phase, which is actually a 2nd stage buffer phase structure. For $0.19 < x < 0.27$, a combination of two phases are detected. With further intercalation ($0.27 < x < 0.56$), the 2nd stage phase (II) disappears and 1st stage (I) single phase structure is observed. The cell parameters increase with the increase of K^+ concentration. During the recharge process, identical phase trans-

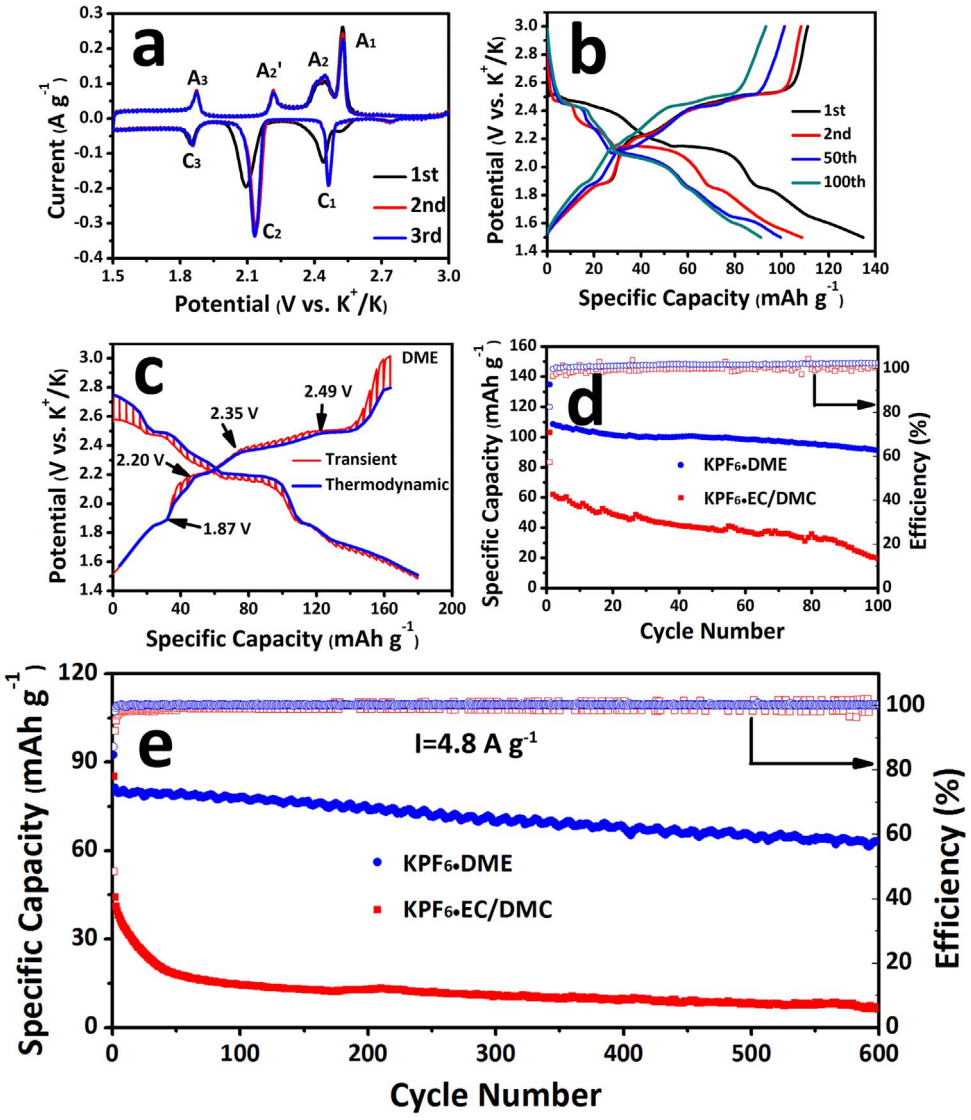

Fig. 2. (a) The first three cyclic voltammetry curves for TiS_2 in DME-based electrolyte at a scan rate of 0.1 mV s^{-1} in 1.5–3.0 V. (b) The galvanostatic discharge-charge curves with different cycles at a current rate of 2 C (480 mA g^{-1}). (c) GITT curves of TiS_2 at the first cycle with a current density of 0.2 C (48 mA g^{-1}) and relaxation time of 20 minutes. (d) Capacity retention behavior comparison as a function of cycling number in ether-based and carbonate-based electrolytes under the same current density of 480 mA g^{-1} in 1.5-3.0 V. (e) Cycling performance of TiS_2 at 20 C (4.8 A g^{-1}).

formations are observed. While the TiS_2 structure is not reversible as it can only be $K_{0.11}TiS_2$ after charged to 3.0 V. We believe the $K_{0.11}TiS_2$ is a thermodynamic stable phase as we have the same results after using a low charge current mode as well as a transient charge mode to avoid the polarizations. This irreversible process absolutely brings in a low initial coulombic efficiency. A chemically pre-potassiating strategy would effectively improve it [17]. The interlay distance in both stage I and stage II structure significantly increases when the potassium atoms get into it. According to the literature of TiS_2 as the lithium ion battery cathode, the Li cations occupy the center of the sulfur atoms to form octahedrons [33]. Nevertheless, the octahedral sites in the van der Waals layer are not enough to accommodate the K cations (radii 1.38 Å *vs.* 0.76 Å of Li^+). As a consequence, the sulfide layers must be separated and the K atoms centered in the sulfur atoms form tetragonal prisms. According to the report of Hibma et al., the separation energy requires a minimum alkali concentration so that there will be a two phase region, but this two phase region can be minimized by the formation of multistage compounds [25]. The K atom intercalation induces the layer distance from 5.70 Å to average of 7.40 Å for the second-stage (II) structure and 8.51 Å for the first-stage (I) structure. The increased distance is larger than the K ion diameter (2.76 Å). This is different from the Na ion intercalation, where the Coulomb forces between the Na with S are stronger than K^+-S^{2-} interactions and the introduction of Na can alleviate the significant repulsions between the sulfurs [25]. Surprisingly, the layer distance without K atoms in the second-stage structure has also expanded from original 5.70 Å to 6.74 Å, implying that the intercalation of K ions induces in-plane electronic structure density rearrangements. The S-S layer separation originating from K intercalation concomitantly brings in the transition metal Ti sliding of 120 degree rotation. In the second-stage structure of $K_{0.11}TiS_2$, the six-fold pattern (c = 44.37 Å = 6 × 7.40 Å) can be reproduced by the 120 degree-rotation of two fold pattern. For the first-stage structure of $K_{0.56}TiS_2$, every three layer restacks into a new periodic layer (c = 25.52 Å = 3 × 8.51 Å). In the way, we can observe a superstructure $\sqrt{3} \times \sqrt{3}$ along the [001] direction besides the 1 × 1 model structure (Fig. 4**d**). It is confirmed by an appearance of equivalent domains rotating 120 ° to each other (Fig. 4**e-f**). Accommodating 0.56 K in every TiS_2 formula leads a liner expansion in the layer distance of 49.2% from 5.70 Å to 8.51 Å. It is larger than 7.25 Å of $Na_{0.55}TiS_2$ [34] as well as larger than typical lithium ion battery cathodes expansion, such as 1.5% for $LiCoO_2$ along c axis [35], −7% in volume for $LiFePO_4$ [36], 0.06% for $LiNi_{0.5}Mn_{1.5}O_4$ along a-

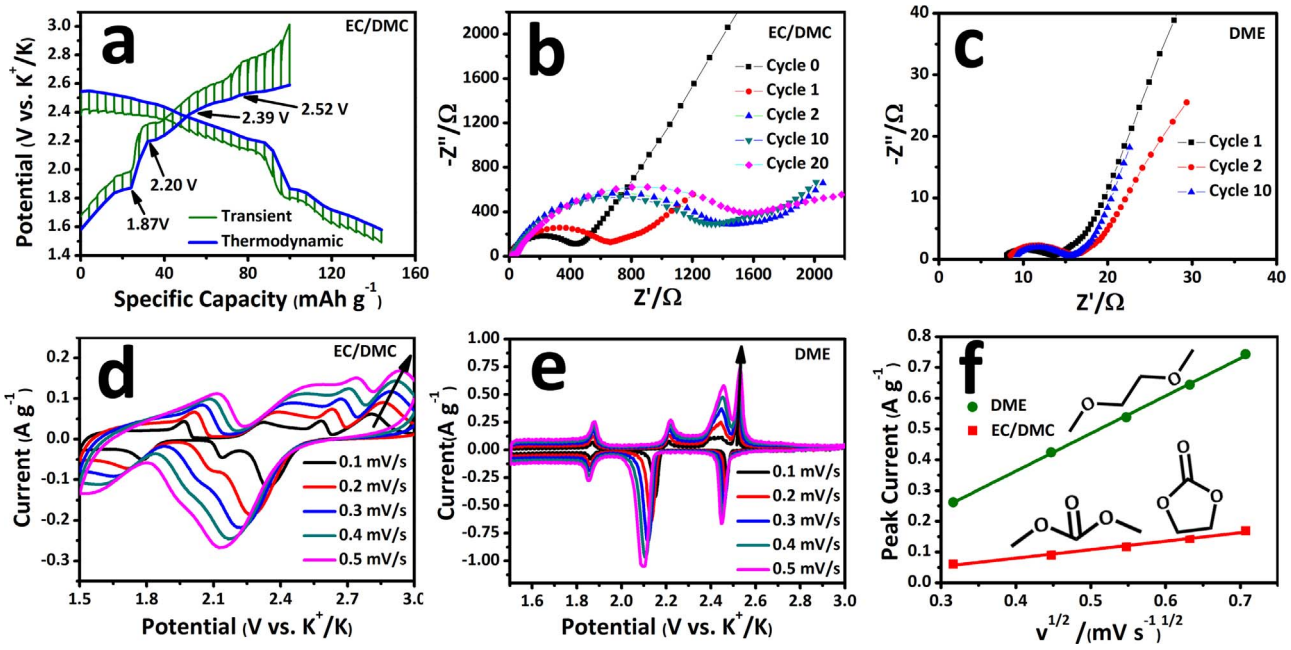

Fig. 3. (a) GITT curves of TiS_2 in EC-DMC KPF_6 electrolyte at the first cycle with a current density of 48 mA g^{-1} and relaxation time of 20 min. (b-c) Electrochemical impedance spectroscopy at different cycles in different electrolytes. Cyclic voltammograms of TiS_2 in DME electrolyte (d) and EC-DMC electrolyte (e) over a scan rate from 0.1 to 0.5 mV s^{-1}. (f) Peak current against square root of scan rate based on (d) and (e).

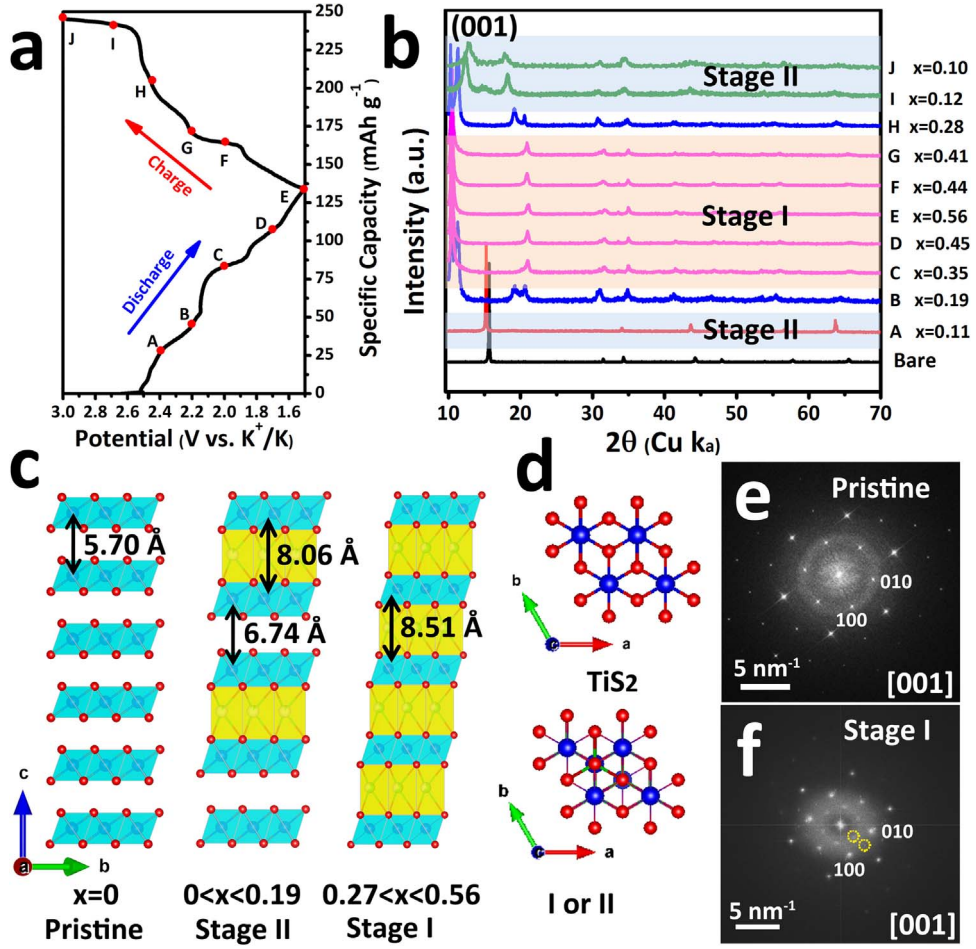

Fig. 4. (a) Galvanostatic discharge-charge curves of TiS_2 for preparing *ex-situ* XRD patterns. (b) Corresponding *ex-situ* XRD patterns. *x* is determined from the capacity. (c) Stage structure evolutions during K intercalation. The Ti, S, and K atoms are denoted by blue, red, green balls, respectively. (d) The crystallographic structures of TiS_2 and Stage I $K_{0.56}TiS_2$ or II $K_{0.11}TiS_2$ along the [001] direction. Supper lattice appearance for K intercalation along [001] direction based on FFT of TEM for TiS_2 (e) and $K_{0.56}TiS_2$ (f). (For interpretation of the references to color in this figure legend, the reader is referred to the web version of this article).

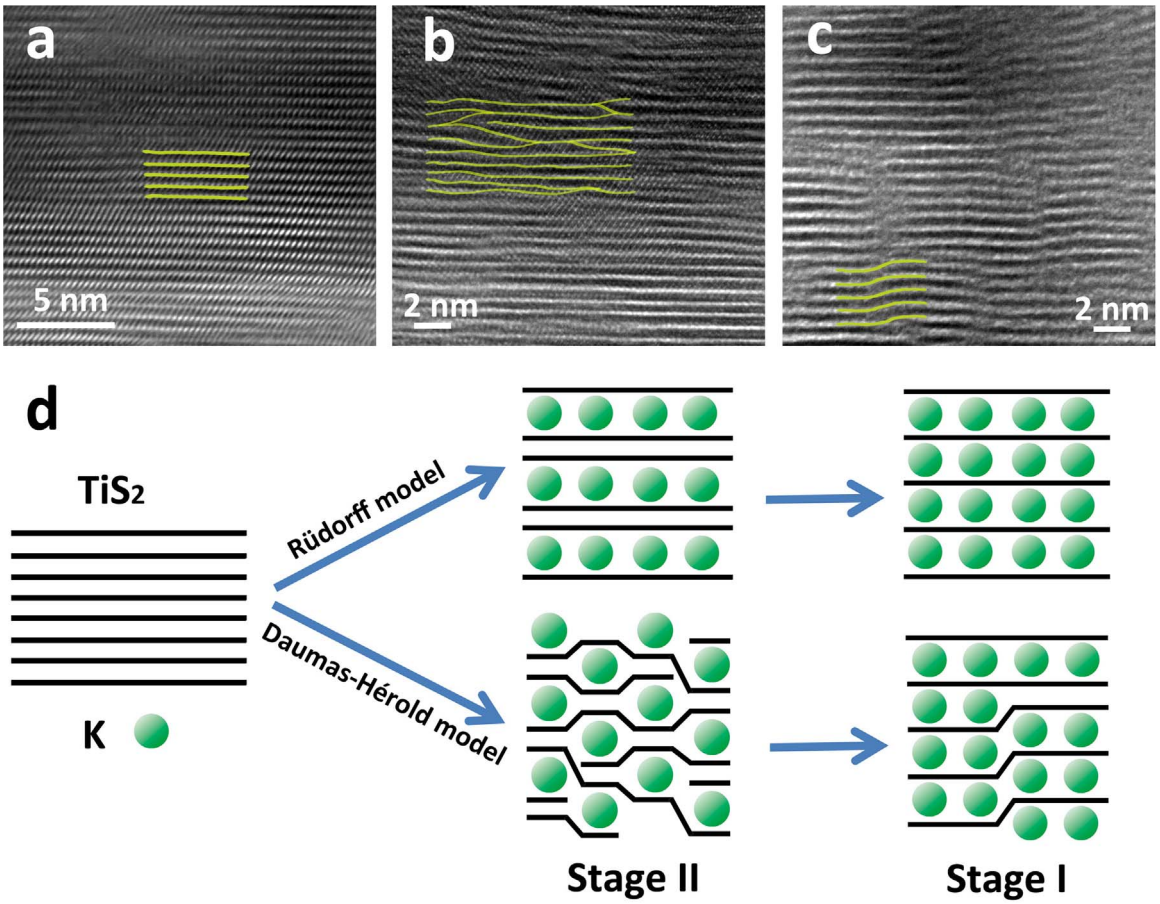

Fig. 5. HRTEM images of the layer distance along (001) plane. (a) TiS_2. (b) 2nd stage structure $K_{0.11}TiS_2$. (c) 1st stage structure $K_{0.56}TiS_2$. (d) Schematic illustrations showing the K intercalation induced stage structure: model proposed by Rüdorff and model proposed by Daumas and Hérold.

axis [37].

X-ray diffraction patterns above give valuable insights into the bulk phase (long-range structure). Here, we import HRTEM to probe the local structure at an atomic level (Fig. 5). Identical results to the XRD patterns, the average (001) lattice distances determined from HRTEM for TiS_2, $K_{0.11}TiS_2$, $K_{0.56}TiS_2$ are 0.57 Å, 0.71 Å, 0.80 Å, respectively. The pristine structure is a well ordered crystalline single phase, while it seems that potassiations in both stage II and Stage I phases result in cracks as demonstrated from the HRTEM images. It can be understood by considering the huge expansion and tensions between fixed and sliding parts of the layers during structure transformations due to the large K ions. Nevertheless, different from the common stage structure sense, also called Rüdorff model that the K atoms strictly intercalate into the TiS_2 layer alternatively, the K atom intercalation forms islands or dislocations in domain size where the K atoms locate in the distorted region. This stage domain model is called Daumas and Hérold model [38]. In this model, the average layer number of intercalating ions for Stage II structure in the macroscopic crystal is two. This domain model can be considered acting as buffer domains to accommodate K cations. Identical phenomena are detected during the other ions intercalation into the layer structures [39].

4. Conclusions

In summary, we have presented that potassium ion battery cathode TiS_2 delivers a superior rate performance with a capacity of 80 mAh g^{-1} at a current rate of 20 C in ether-type electrolyte. Although it has the same intercalation mechanism with that in the carbonate-based electrolyte system evidenced by GITT technique, the ether electrolytes provide better kinetics in charge transfer rate and apparent K cation diffusion coefficient. The potassium interaction into the TiS_2 frameworks to be K_xTiS_2 undergoes a second-stage structure ($0 < x < 0.19$) and a first-stage structure ($0.27 < x < 0.60$) in the voltage window 1.5-3.0 V, in between a two-phase combination. The K atoms centered in the sulfur atoms formed tetragonal prisms accompanied with a S-S layer separation and Ti-S sliding with a rotation of 120° leading a commensurate superstructure $\sqrt{3} \times \sqrt{3}$ in addition to the 1×1 of pristine TiS_2 framework. High resolution TEM proves a Daumus-Hérold model for the stage structure instead of the Rüdorff model. This study addresses the importance of electrolytes in improving electrochemical properties in potassium ion batteries and enriches the knowledge of intercalations chemistry with large alkaline metal ions.

Acknowledgements

This work is supported by the National Natural Science Foundation of China (51502032, 11327902, 51725206, 51502007, 51672007, 21673033, 11234013, 21473022) and the Fundamental Research Funds for the Central Universities, China (No. ZYGX2016J044). The authors acknowledge the Electron Microscopy Laboratory in Peking University for the use of Cs corrected electron microscope.

Appendix A. Supporting information

Supplementary data associated with this article can be found in the online version at doi:10.1016/j.ensm.2017.12.018.

References

[1] J. Liang, F. Li, H.-M. Cheng, On energy: batteries beyond lithium ion, Energy Storage Mater. 7 (2017) A1–A3.
[2] Y. Wang, R. Chen, T. Chen, H. Lv, G. Zhu, L. Ma, C. Wang, Z. Jin, J. Liu, Emerging non-lithium ion batteries, Energy Storage Mater. 4 (2016) 103–129.
[3] A. Eftekhari, Z. Jian, X. Ji, Potassium secondary batteries, ACS Appl. Mater. Interfaces 9 (2016) 4404–4419.
[4] Q. Deng, J. Pei, C. Fan, J. Ma, B. Cao, C. Li, Y. Jin, L. Wang, J. Li, Potassium salts of para-aromatic dicarboxylates as the highly efficient organic anodes for low-cost K-ion batteries, Nano Energy 33 (2017) 350–355.
[5] G. Yoon, H. Kim, I. Park, K. Kang, Conditions for reversible Na intercalation in graphite: theoretical studies on the interplay among guest ions, solvent, and graphite host, Adv. Energy Mater. 7 (2017) 1601519–1611528.
[6] N. Matsuura, K. Umemoto, Zi Takeuchi, Standard potentials of alkali metals, silver, and thallium metal/ion couples in N, N′-dimethylformamide, dimethyl sulfoxide, and propylene carbonate, Bull. Chem. Soc. Jpn. 47 (1974) 813–817.
[7] Z. Jian, W. Luo, X. Ji, Carbon electrodes for K-ion batteries, J. Am. Chem. Soc. 137 (2015) 11566–11569.
[8] Z. Jian, Z. Xing, C. Bommier, Z. Li, X. Ji, Hard carbon microspheres: potassium-ion anode versus sodium-ion anode, Adv. Energy Mater. 6 (2016) 1501874–1501879.
[9] C. Chen, Z. Wang, B. Zhang, L. Miao, J. Cai, L. Peng, Y. Huang, J. Jiang, Y. Huang, L. Zhang, Nitrogen-rich hard carbon as a highly durable anode for high-power potassium-ion batteries, Energy Storage Mater. 8 (2017) 161–168.
[10] A. Eftekhari, Potassium secondary cell based on Prussian blue cathode, J. Power Sources 126 (2004) 221–228.
[11] C. Vaalma, G.A. Giffin, D. Buchholz, S. Passerini, Non-aqueous K-ion battery based on layered $K_{0.3}MnO_2$ and hard carbon/carbon black, J. Electrochem. Soc. 163 (2016) A1295–A1299.
[12] J. Han, G.-N. Li, F. Liu, M. Wang, Y. Zhang, L. Hu, C. Dai, M. Xu, Investigation of $K_3V_2(PO_4)_3$/C nanocomposites as high-potential cathode materials for potassium-ion batteries, Chem. Commun. 53 (2017) 1805–1808.
[13] X. Sun, P. Bonnick, L.F. Nazar, Layered TiS_2 positive electrode for Mg batteries, ACS Energy Lett. 1 (2016) 297–301.
[14] A. Lerf, R. Schöllhorn, Solvation reactions of layered ternary sulfides A_xTiS_2, A_xNbS_2, and A_xTaS_2, Inorg. Chem. 16 (1977) 2950–2956.
[15] P. Gao, L. Wang, Y. Zhang, Y. Huang, K. Liu, Atomic-scale probing of the dynamics of sodium transport and intercalation-induced phase transformations in MoS_2, ACS Nano 9 (2015) 11296–11301.
[16] P. Gao, L. Wang, Y.-Y. Zhang, Y. Huang, L. Liao, P. Sutter, K. Liu, D. Yu, E.-G. Wang, High-resolution tracking asymmetric lithium insertion and extraction and local structure ordering in SnS_2, Nano Lett. 16 (2016) 5582–5588.
[17] B. Tian, W. Tang, K. Leng, Z. Chen, S.J.R. Tan, C. Peng, G.-H. Ning, W. Fu, C. Su, G.W. Zheng, Phase transformations in TiS_2 during K intercalation, ACS Energy Lett. 2 (2017) 1835–1840.
[18] D. Aurbach, Y. Ein-Eli, The study of Li-graphite intercalation processes in several electrolyte systems using in situ X-ray diffraction, J. Electrochem. Soc. 142 (1995) 1746–1752.
[19] Y. Liu, L. Wang, L. Cao, C. Shang, Z. Wang, H. Wang, L. He, J. Yang, H. Cheng, J.Z. Li, Understanding and suppressing side reactions in Li-air batteries, Mater. Chem. Front. 1 (2017) 2495–2510.
[20] H. Kim, K. Lim, G. Yoon, J.H. Park, K. Ku, H.D. Lim, Y.E. Sung, K. Kang, Exploiting lithium-ether Co-intercalation in graphite for high-power lithium-ion batteries, Adv. Energy Mater. 7 (2017) 1700418.
[21] H. Pan, J. Chen, R. Cao, V. Murugesan, N.N. Rajput, K.S. Han, K. Persson, L. Estevez, M.H. Engelhard, J.-G. Zhang, Non-encapsulation approach for high-performance Li-S batteries through controlled nucleation and growth, Nat. Energy 2 (2017) 813–820.
[22] Z. Jian, Y. Liang, I.A. Rodríguez-Pérez, Y. Yao, X. Ji, Poly (anthraquinonyl sulfide) cathode for potassium-ion batteries, Electrochem. Commun. 71 (2016) 5–8.
[23] K. Lei, F. Li, C. Mu, J. Wang, Q. Zhao, C. Chen, J. Chen, High K-storage performance based on the synergy of dipotassium terephthalate and ether-based electrolytes, Energy Environ. Sci. 10 (2017) 552–557.
[24] H. Starnberg, Recent developments in alkali metal intercalation of layered transition metal dichalcogenides, Mod. Phys. Lett. 14 (2000) 455–471.
[25] T. Hibma, X-ray study of the ordering of the alkali ions in the intercalation compounds Na_xTiS_2 and Li_xTiS_2, J. Solid State Chem. 34 (1980) 97–106.
[26] M.S. Whittingham, Electrical energy storage and intercalation chemistry, Science 192 (1976) 1126–1127.
[27] X. Ren, Q. Zhao, W.D. McCulloch, Y. Wu, MoS_2 as a long-life host material for potassium ion intercalation, Nano Res. 4 (2017) 1313–1321.
[28] J. Han, Y. Niu, S.-j Bao, Y.-N. Yu, S.-Y. Lu, M. Xu, Nanocubic $KTi_2(PO_4)_3$ electrodes for potassium-ion batteries, Chem. Commun. 52 (2016) 11661–11664.
[29] N. Recham, Gl Rousse, M.T. Sougrati, J.-Nl Chotard, C. Frayret, S. Mariyappan, B.C. Melot, J.-C. Jumas, J.-M. Tarascon, Preparation and characterization of a stable $FeSO_4F$-based framework for alkali ion insertion electrodes, Chem. Mater. 24 (2012) 4363–4370.
[30] H. Kim, J.C. Kim, S.H. Bo, T. Shi, D.H. Kwon, G. Ceder, K-ion batteries based on a P2-type $K_{0.6}CoO_2$ cathode, Adv. Energy Mater. 7 (2017) 1700098–1700106.
[31] X. Dai, L. Wang, J. Xu, Y. Wang, A. Zhou, J. Li, Improved electrochemical performance of $LiCoO_2$ electrodes with ZnO coating by radio frequency magnetron sputtering, ACS Appl. Mater. Interfaces 6 (2014) 15853–15859.
[32] H.-D. Lim, B. Lee, Y. Bae, H. Park, Y. Ko, H. Kim, J. Kim, K. Kang, Reaction chemistry in rechargeable Li-O_2 batteries, Chem. Soc. Rev. 46 (2017) 2873–2888.
[33] J. Dahn, W. McKinnon, R. Haering, W. Buyers, B. Powell, Structure determination of Li_xTiS_2 by neutron diffraction, Can. J. Phys. 58 (1980) 207–213.
[34] K. Cenzual, L.M. Gelato, M. Penzo, E. Parthe, Inorganic structure types with revised space-groups.I*, Acta Cryst. B47 (1991) 433–439.
[35] X. Lu, Y. Sun, Z. Jian, X. He, L. Gu, Y.-S. Hu, H. Li, Z. Wang, W. Chen, X. Duan, New insight into the atomic structure of electrochemically delithiated O3-$Li_{(1-x)}CoO_2$ ($0 \le x \le 0.5$) nanoparticles, Nano Lett. 12 (2012) 6192–6197.
[36] O. Haas, A. Deb, E. Cairns, A. Wokaun, Synchrotron X-ray absorption study of $LiFePO_4$ electrodes, J. Electrochem. Soc. 152 (2005) A191–A196.
[37] L. Wang, H. Li, X. Huang, E. Baudrin, A comparative study of Fd-3m and $P4_332$ "$LiNi_{0.5}Mn_{1.5}O_4$", Solid State Ion. 193 (2011) 32–38.
[38] N. Daumas, A. Herold, Relations between phase concept and reaction mechanics in graphite insertion compounds, C. R. Acad. Sci. 268 (1969) 373–382.
[39] A.M. Fogg, J.S. Dunn, D. O'Hare, Formation of second-stage intermediates in anion-exchange intercalation reactions of the layered double hydroxide $[LiAl_2(OH)_6]Cl{\cdot}H_2O$ as observed by time-resolved, in situ x-ray diffraction, Chem. Mater. 10 (1998) 356–360.